JACS JOURNAL OF THE AMERICAN CHEMICAL SOCIETY

Article

Cite This: J. Am. Chem. Soc. 2019, 141, 981−989

pubs.acs.org/JACS

Triarylmethane Fluorophores Resistant to Oxidative Photobluing

Alexey N. Butkevich,*[,†,‡] Mariano L. Bossi,[‡] Gražvydas Lukinavičius,[†] and Stefan W. Hell*[,†,‡]

[†]Department of NanoBiophotonics, Max Planck Institute for Biophysical Chemistry, Am Fassberg 11, 37077 Göttingen, Germany

[‡]Department of Optical Nanoscopy, Max Planck Institute for Medical Research, Jahnstrasse 29, 69120 Heidelberg, Germany

Supporting Information

ABSTRACT: Spectral stability of small-molecule fluorescent probes is required for correct interpretation and reproducibility of multicolor fluorescence imaging data, in particular under high (de)excitation light intensities of super-resolution imaging or in single-molecule applications. We propose a synthetic approach to a series of spectrally stable rhodamine fluorophores based on sequential Ru- and Cu-catalyzed transformations, evaluate their stability against photobleaching and photoconversion in the context of other fluorophores using chemometric analysis, and demonstrate chemical reactivity of fluorophore photoproducts. The substitution patterns providing the photoconversion-resistant triarylmethane fluorophores have been identified, and the applicability of nonbluing labels in live-cell STED nanoscopy is demonstrated.

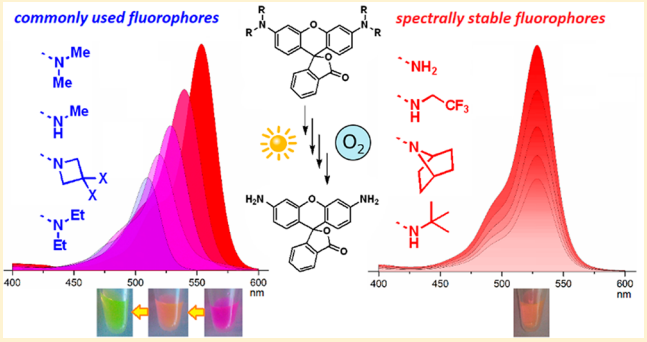

INTRODUCTION

With the recent developments of fluorescence nanoscopy (super-resolution microscopy) methods,[1] it has now become possible to observe and study nanoscale structures on the cell surface[2] and within the cell interior[3] with the help of advanced optical microscopes. The observation of real-time interactions between individual (labeled) biomolecules in living cells and tissues over extended periods of time is of particular value to life sciences.[4] For simultaneous selective detection and localization of multiple distinct light-emitting species using optical techniques, clear differentiation of their photophysical or photochemical behavior is prerequisite. The most straightforward approach, multiplexing by excitation or emission wavelength, permits encoding multiple colors in fluorescence nanoscopy using suitable fluorophores. It is, however, limited by the intrinsically broad nature of excitation and emission spectra of most common fluorophores (around 50 nm at half-maximum). Even under these constraints, we have recently realized three-color STED nanoscopy in living cells using fluorescent labels with well separated excitation and emission maxima ($\Delta\lambda_{max} \geq 60$ nm) with a commercial microscope.[5] Using a custom hyperspectral detection setup and labels with overlapping absorption and emission spectra ($\Delta\lambda_{max} \sim 30$ nm), super-resolution STED imaging with four color channels was made possible.[6]

Sophisticated color separation techniques in fluorescence microscopy, such as spectrally resolved fluorescence lifetime imaging,[7] and signal processing methods including spectral unmixing, deconvolution, and demodulation,[8] rely heavily on the spectral stability of the employed fluorescent labels. However, all organic fluorophores to different extents are prone to the detrimental processes of photobluing or photoredding (i.e., hypso- or bathochromic shift, respectively, of excitation and fluorescence emission maxima of fluorophore photoproducts) as well as blinking[9] (transient conversion into nonemissive states or species) and photobleaching[10] (irreversible degradation of the fluorophore). These processes are particularly consequential in the presence of oxidizing (dissolved oxygen) and reducing species (glutathione and nicotinamide adenine dinucleotide phosphate), which are naturally abundant in eukaryotic cells.[11] While blinking and bleaching typically result in the loss of signal intensity and resolution in fluorescence nanoscopy methods, spectral instability of fluorescent markers (their bluing or redding) will lead to misidentification of individual labels and obfuscation of the resulting multicolor data due to inconsistent crosstalk levels between the excitation or detection channels. Spectral stability of labels under demanding conditions of fluorescence nanoscopy (high intensities of excitation or de-excitation light), particularly in live samples where the concentration levels of molecular oxygen cannot be controlled, is therefore essential for the integrity of the collected multicolor data.

While fluorophore brightness[12] and its resistance against photobleaching[13] with regard to cell imaging applications have been addressed in several reports, no studies so far have specifically focused on the problem of spectral instability of fluorescent labels. In the present work, we quantify the prevalence of the photobluing phenomenon and propose possible solutions pertaining to development of widely used triarylmethane fluorophores.

Received: October 12, 2018
Published: December 18, 2018

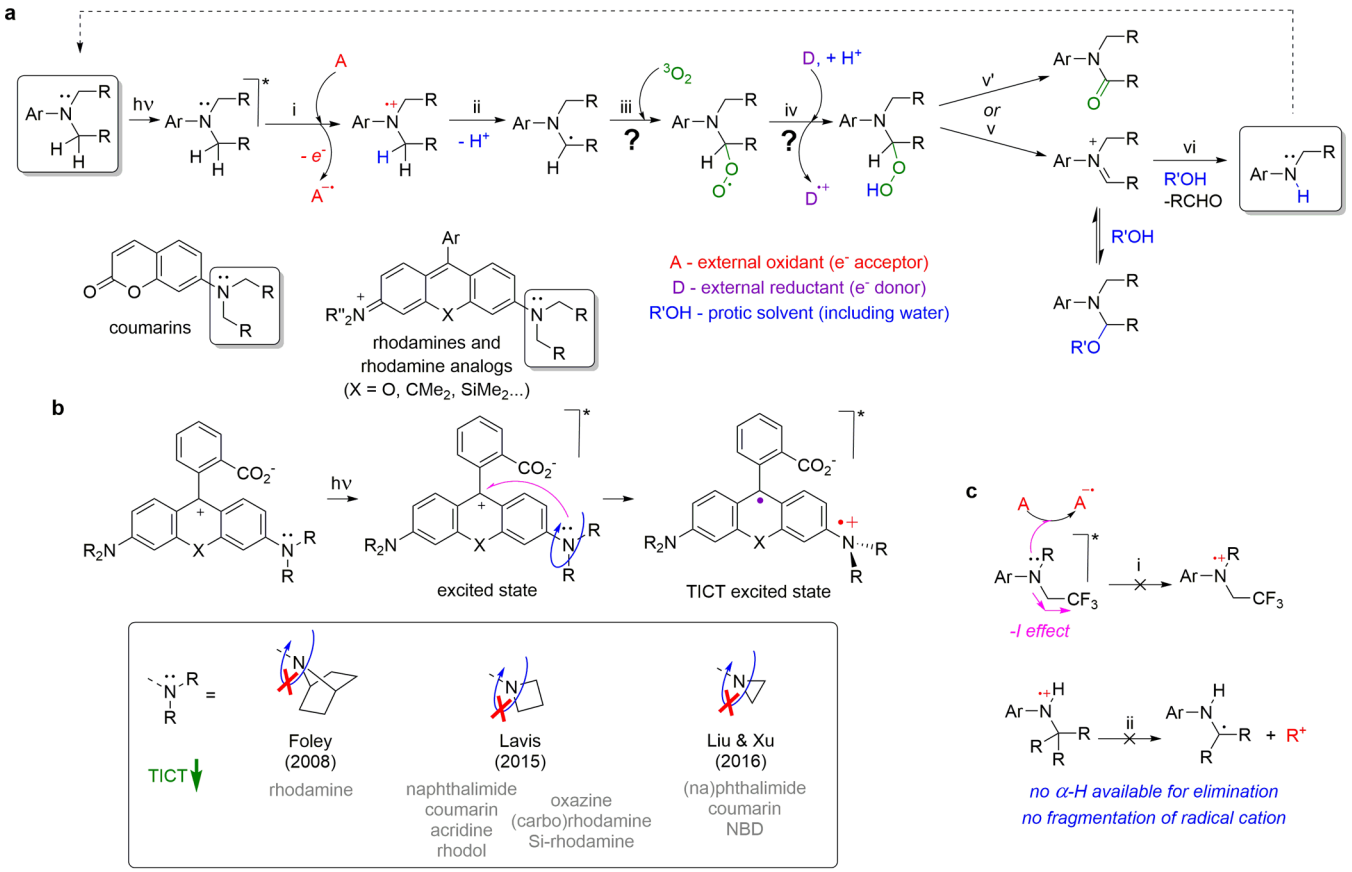

Figure 1. (a) General oxidative photobluing pathway for fluorescent dyes with (di)alkylamino auxochromic groups. (b) Strategies aimed at suppression of transitioning into the twisted intramolecular charge transfer (TICT) excited state for select classes of fluorophores; NBD − 4-nitro-2,1,3-benzoxadiazole. (c) Possible approaches to mitigate the dye photobluing unrelated to TICT suppression. Question marks denote the steps with possible participation of other redox partners.

Stepwise photooxidative *N*-dealkylation of rhodamines, leading to hypsochromic shifts of their absorption and emission maxima (10−15 nm per single dealkylation step), has been known for over 40 years.[14] Similar processes have been reported for other triarylmethane dyes[15] and 7-(dialkylamino)coumarins.[16] The oxidative dealkylation of tertiary amines proceeds through the initial formation of a radical cation, which is deprotonated to form an α-aminoalkyl radical. In oxygen-containing media, the latter loses an alkyl substituent in the form of an aldehyde through the intermediacy of a hemiaminal, peroxyhemiaminal, or iminium-type species (assuming for simplicity the absence of other oxidants; Figure 1a). Similar reactivity was observed upon electrochemical[17] or photocatalytic[18] oxidation of tertiary amines. Formation of chemically stable photoredding products is much more uncommon; however photooxidation of an *N*,*N*-diethylamino substituent into the corresponding *N*-ethylacetamide imposing a spectral red shift has been demonstrated for a trioxatriangulenium dye.[19] On the contrary, similar α-oxidation of the dialkylamine fragment of coumarin 153 resulted in regioisomeric amide photoproducts with blue-shifted absorption maxima.[20]

Related to the oxidative photodealkylation process described above is the transition of a fluorophore into a twisted intramolecular charge transfer (TICT) excited state, which in the case of triarylmethane dyes corresponds to an internal electron transfer from a (di)alkylamino substituent to the xanthylium core. As the ensuing amine radical cation can undergo similar *N*-dealkylation, the suppression of the TICT pathway, besides the improved photostability and fluorescence quantum yield, will also reduce photobluing. This approach was first introduced by Foley[21] and later developed by Lavis[12b] and Liu and Xu[22] who proposed, respectively, to substitute the freely rotating *N*,*N*-dialkylamino groups in rhodamine-type fluorophores with bridged 7-azabicyclo[2.2.1]heptane, azetidine, or aziridine substituents (Figure 1b).

Other than TICT suppression, it is evident from the mechanism of oxidative photodealkylation (Figure 1a) that hindering either the first (one-electron photooxidation, step i) or the second step (α-deprotonation of the radical cation, step ii) of the oxidative cycle should prevent fluorophore photobluing (Figure 1c). The former can, in principle, be achieved with the introduction of electron-withdrawing groups, such as 2,2,2-trifluoroethyl, as amine substituents. Indeed, many fluorinated rhodamines[23] and carborhodamines[24] have already been employed as photostable labels for live and fixed-cell STED imaging. The most straightforward way to avoid α-deprotonation in step ii would be to introduce *tert*-alkyl substituents lacking α-hydrogen atoms, which is the approach of the present work.

RESULTS AND DISCUSSION

Synthesis and Characterization of *N*,*N*′-Di-*tert*-alkylrhodamines. To evaluate the photobluing resistance of *N*,*N*′-di-*tert*-alkylrhodamines, we had first to address the problem of their synthetic accessibility. The shortest approach to

DOI: 10.1021/jacs.8b11036
J. Am. Chem. Soc. 2019, 141, 981−989

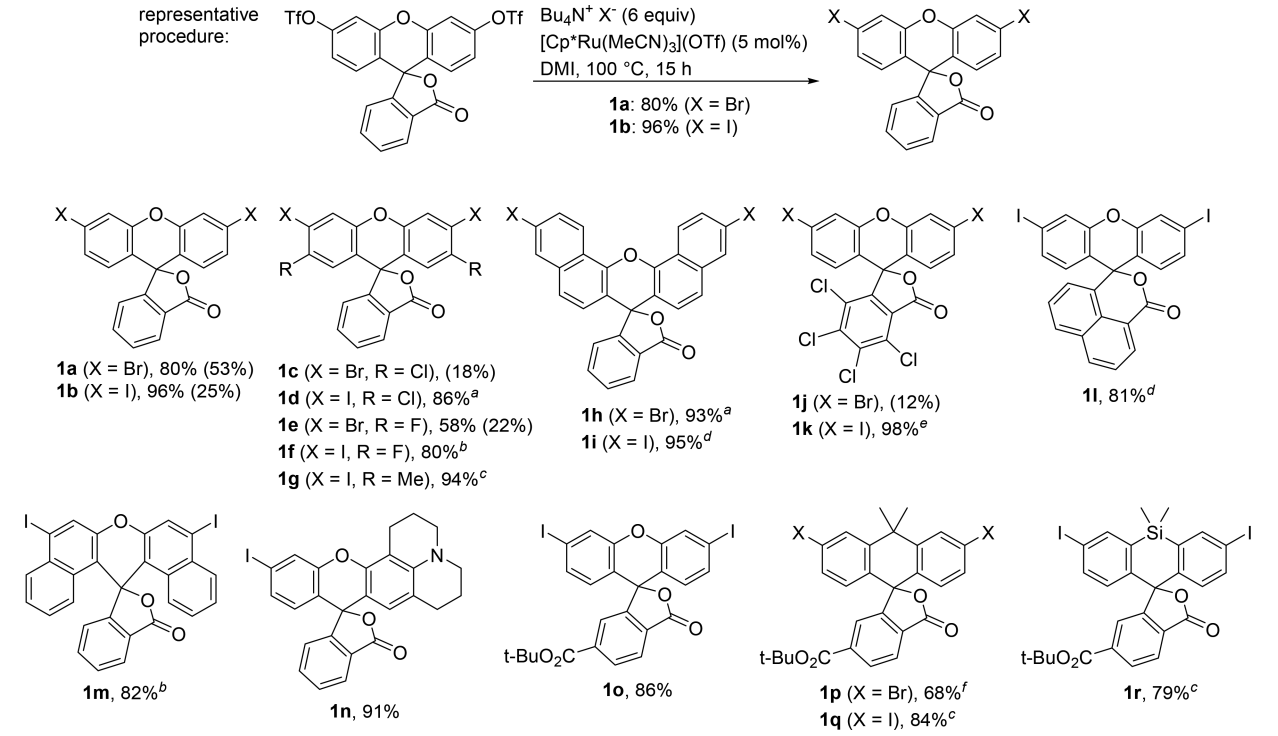

Figure 2. Ru-catalyzed synthesis of 3′,6′-dihalofluorans: (a) with 10 mol % [Ru]; (b) with 5 mol % $[Cp^*RuCl_2]_n$; (c) with 10 mol % [Ru], reaction time 38 h; (d) with 10 mol % $[Cp^*RuCl_2]_n$; (e) at 120 °C, reaction time 16 h; (f) LiBr was used instead of Bu_4NBr. DMI − 1,3-dimethyl-2-imidazolidinone. The yields in parentheses correspond to the acid-mediated condensation between the corresponding phthalic anhydride and 3-halophenol (neat methanesulfonic acid, 140−150 °C, 20−40 h).

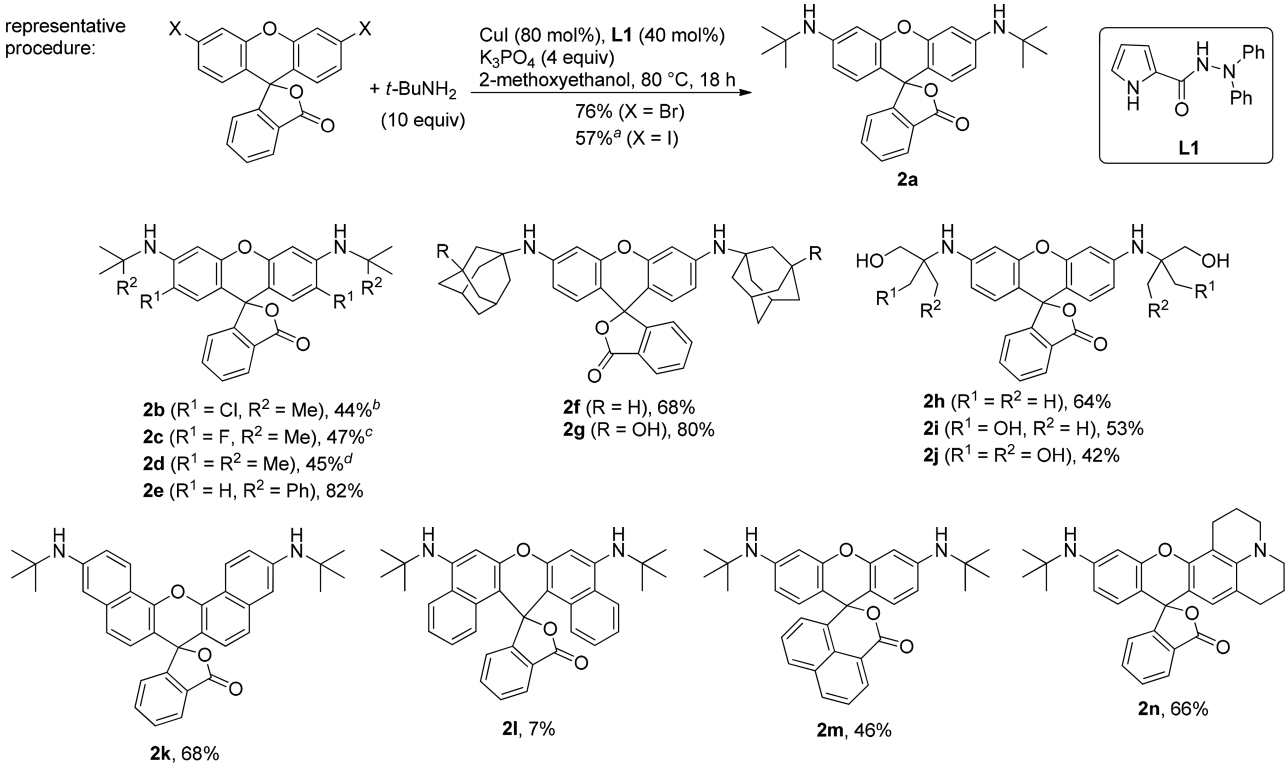

Figure 3. Synthesis of *N*,*N*′-di-*tert*-alkylrhodamines by Ullmann-type amination of 3′,6′-dihalofluorans: (a) 66% yield with 20 mol % CuI and 20 mol % **L1**; (b) at 50 °C, reaction time 68 h; (c) at 50 °C, reaction time 63 h; (d) reaction time 40 h.

symmetric triarylmethane dyes offering the highest *N*-substituent diversity has so far been the double Buchwald−Hartwig amination of fluorescein ditriflates, proposed by Grimm and Lavis.[25] These triflates, however, are rather poor substrates for amination, as can be seen from the necessity of using high catalyst loads (typically 20 mol % of Pd source and

DOI: 10.1021/jacs.8b11036
J. Am. Chem. Soc. 2019, 141, 981−989

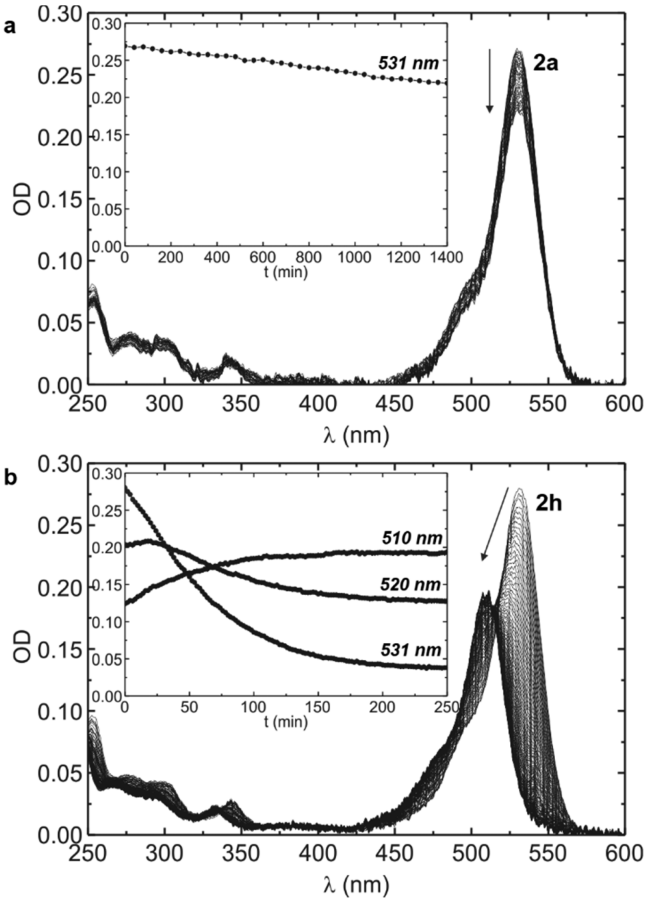

Figure 4. Time-resolved absorption spectroscopy experiment demonstrating photolysis of (a) a photooxidation-resistant, nonbluing fluorophore **2a** in comparison with (b) a photooxidation-prone fluorophore **2h** in 0.1% (v/v) TFA–ethanol. The insets show the absorption transients at the absorption λ_{max} of 531 nm (a) and 531, 520, and 510 nm (b), corresponding to the absorption maxima of the starting materials and photoproducts. OD = optical density of solution at a given wavelength λ, optical path l = 1 cm.

30 mol % of mono- or bis-phosphine ligand) and Cs_2CO_3 base to achieve satisfactory preparative yields. To highlight these difficulties, and despite the fact that in recent years several highly active catalytic systems have been proposed specifically for Pd- and Ni-catalyzed arylation of hindered primary amines[26] and base-sensitive substrates,[27] in our test reactions we have failed to obtain the coupling product between fluorescein ditriflate and *tert*-butylamine (**2a**) with acceptable yield (see Table S1). Instead, net hydrolysis of the triflate was invariably the overwhelming pathway.

This setback led us to consider the Ullmann reaction as a possible alternative for the synthesis of *N*,*N*′-di-*tert*-alkylrhodamines. The copper-catalyzed amination of aryl halides has the advantage of operating along a different mechanistic pathway, being more tolerant to the nature of solvent and substrate than Pd- and Ni-catalyzed coupling reactions, and employing an abundant metal and usually inexpensive ligands.[28] Aryl sulfonates, however, are known to be unsuitable partners for Ullmann-type reactions, as a halide leaving group, preferably a bromide or iodide, is required. We had therefore to meet a twofold challenge of securing access to diversely substituted 3′,6′-dihalofluorans and realizing a double Ullmann amination on these substrates with primary or secondary *tert*-alkylamines.

Gratifyingly, the required transformation of aryl triflates to aryl bromides or iodides has been reported,[29] and with minor modifications, we found it perfectly suitable for the transformation of fluorescein, carbo- and silicofluorescein ditriflates, and rhodol triflates to the corresponding halofluorans (Figure 2). The originally employed cationic Ru(II) catalyst [Cp*Ru(MeCN)$_3$]OTf could in many cases be replaced with a less expensive Ru(III) precatalyst[30] $[Cp^*RuCl_2]_n$. On the contrary, the corresponding Rh(III) complex $[Cp^*Rh(MeCN)_3](SbF_6)_2$ was found to be completely ineffective (Table S2), and Grushin's catalyst[31] $[Cp^*Ru(\eta^6\text{-}C_{10}H_8)]BF_4$, presumably operating through a nucleophilic substitution in a η^6-coordinated Ru(II)-arene π-complex,[32] was much less active. The hygroscopic LiBr and NaI salts were substituted with Bu_4NBr and Bu_4NI, which allowed the reaction to be set up in open air.

Besides fluorescein triflates, the corresponding fluorosulfonates and nonaflates (less reactive) could be employed as the starting materials. Other more electron-rich sulfonates (fluorescein dimesylate and ditosylate) did not participate in the transformation, resulting in nearly complete recovery of the starting material. Ortho-substituted or otherwise sterically hindered aryl triflates were well tolerated but required longer reaction times and/or higher catalyst loads (see Figure 2 and SI), and no halide scrambling was observed with F- or Cl-substituted (but not with Br-substituted) 3′,6′-diiodofluoran. It is worth noting that the mild reaction conditions and broad substrate tolerance of the Ru-catalyzed synthesis of 3′,6′-dihalofluorans are particularly evident when compared to the classic condensation of 3-halophenols with phthalic anhydride in neat strong acid (see the SI). As a result, only a few simple halofluorans, and none of their group 14 atom-bridged analogues, have been previously accessed.

In a recent work by Zhu and Wan,[33] an Ullmann-type amination of aryl bromides and iodides with secondary and primary amines, including 1-aminoadamantane, under exceptionally mild conditions (5 mol % of Cu catalyst, K_3PO_4 base in diethylene glycol, rt to 60 °C) has been reported. Employing this catalytic system, upon optimization (Table S3) we were able to achieve double amination with primary *N*-*tert*-alkylamines on a diverse variety of 3′,6′-dibromo- and 3′,6′-diiodofluorans prepared as described above (Figure 3). Under high catalyst loads (40 mol % **L1**, 80 mol % CuI) and with mild heating (80 °C), it was possible to suppress the side reactions (mainly Cu-catalyzed solvolysis of aryl halides) and reach practicable preparative yields. Both an alcohol solvent (2-methoxyethanol was preferred over diethylene glycol owing to its lower boiling point) and the use of a bidentate ligand with a pyrrole-type nitrogen in the 2-position to a carbohydrazide or carbohydroxamate moiety were required (Table S3). Multiple unprotected hydroxyl groups in the amine substituent were well tolerated if aryl iodides were used as the coupling partners. However, further increasing the steric bulk of *tert*-alkylamines (in the cases of 2,2,6,6-tetramethylpiperidine, 2-(*tert*-butylamino)ethanol, or tritylamine) completely shut down their reactivity.

The photophysical properties of *N*,*N*′-di-*tert*-alkylrhodamines are compiled in Table S4. For comparative evaluation of photostability and brightness of the new fluorophores, a series of reference rhodamine dyes (TMR, JF_{525}, JF_{549}, **3a**–**d**) have also been prepared (Table S5). We found that *N*,*N*′-di-*tert*-alkylrhodamines are generally bright fluorophores ($\varepsilon \sim 1 \times 10^5$ M^{-1} cm^{-1}, fluorescence quantum yields >90%) with

DOI: 10.1021/jacs.8b11036
J. Am. Chem. Soc. 2019, 141, 981–989

Table 1. Photobleaching and Photobluing Quantum Yields for a Series of Nonbluing vs Bluing Rhodamine Fluorophores*

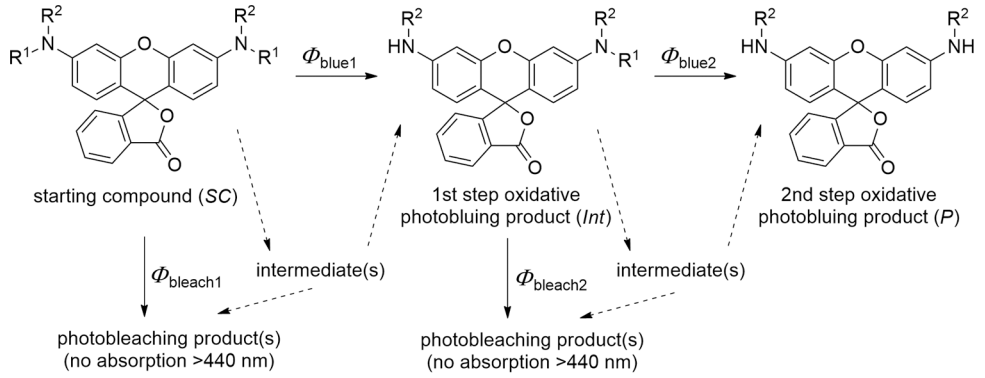

	Fluorophore	Φ_{blue1}, $\times10^{-6}$	Φ_{blue2}, $\times10^{-6}$	$\Phi_{bleach1}$, $\times10^{-6}$	$\Phi_{bleach2}$, $\times10^{-6}$	$\Phi_{blue1}+\Phi_{bleach1}$, $\times10^{-6}$	$\Phi_{blue1}/\Phi_{bleach1}$
Non-bluing fluorophores	**2e**	–	–	0.0097	–	0.0097	0
	2g	–	–	0.066	–	0.066	0
	2f	–	–	0.093	–	0.093	0
	3d	–	–	0.13	–	0.13	0
	2a	–	–	0.14	–	0.14	0
	3c	–	–	0.14	–	0.14	0
	Rhodamine 110	–	–	0.14	–	0.14	0
	2d	–	–	0.16	–	0.16	0
	2m	–	–	0.19	–	0.19	0
	2c	–	–	0.28	–	0.28	0
Bluing fluorophores	JF_{549}	0.28	n.o.[a]	0.27	0.31	0.54	1.0
	TMR	0.5	n.o.	0.083	0.43	0.58	6.0
	JF_{525}	0.21	n.o.	0.51	n.o.	0.72	0.41
	Rhodamine B	0.63	n.o.	0.14	0.42	0.76	4.5
	3a	–[b]	–[b]	0.72	–	0.72	–[b]
	Rhodamine 6G	1.9	0.46	0.5	0.44	2.4	3.8
	2j	2.0	2.0	0.67	0.19	2.7	3.0
	3b	0.28	n.o.	2.7	n.o.	3.0	0.10
	2i	6.2	4.6	1.5	2.5	7.7	4.1
	2h	29	21	4.3	5.3	33	6.7

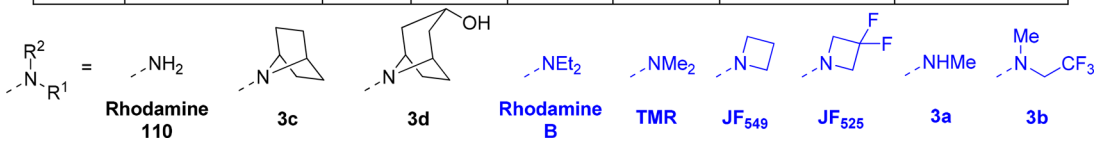

*Simplified scheme of the two-step oxidative photobluing of a rhodamine fluorophore (assuming either $R^1 = R^2$, R^2 = H, or much higher photooxidation rate for R^1 substituent; for more complex cases, see SI) with concomitant photobleaching. Φ denotes a calculated quantum yield for the corresponding photochemical process based on the optimized absorption spectra matrix fit (see SI). The fluorophores within each group are listed from highest to lowest photostability (increasing $\Phi_{blue1} + \Phi_{bleach1}$). [a]n.o.: not observed within the time frame of the experiment. [b]Complex mechanism with accumulation of multiple products; the data were fitted at low photoconversion (ca. < 15%), where photobleaching was the main observed process.

excited-state lifetimes of up to 4 ns and are spectrally similar to *N*,*N*′-dialkylrhodamines such as 520R[24a] or Rhodamine 6G. Unlike the latter, the dyes **2b**–**d**, bearing substituents ortho to the amino groups, manifest significantly lower quantum yields.

Photophysical Properties and Photooxidative Degradation of Rhodamine Fluorophores. With the demonstrated robustness of the proposed synthetic approach, we moved on to evaluate the photostability of *N*,*N*′-di-*tert*-alkylrhodamines in relation to other known rhodamine fluorophores (**3a**,**b**, TMR, Rhodamines 110, B, 6G and relevant Janelia Fluor dyes). Our intent was to compare the relative photobleaching and photobluing rates for different substitution patterns. To this end, dilute (~10 μM) solutions of the tested fluorophores in air-saturated acidified ethanol (with 0.1 v/v% TFA) were continuously irradiated (see the SI) with intermittent recording of absorption spectra (Figure 4). The resulting kinetic data were passed to an iterative fitting procedure[34] calculating the quantum yields of the individual photoprocesses according to a simplified general mechanism including up to two consecutive photobluing steps (Table 1). To ensure the correct interpretation of the spectroscopic data and identification of the photoproducts, a series of photolyses have been performed on a semipreparative scale (~50 μmol) in a custom-built flow photoreactor (Figures S2–S22), and the photoproducts were unambiguously identified by (HR-)MS, NMR, and UV–vis spectrometry (Tables S6–S12).

DOI: 10.1021/jacs.8b11036
J. Am. Chem. Soc. 2019, 141, 981–989

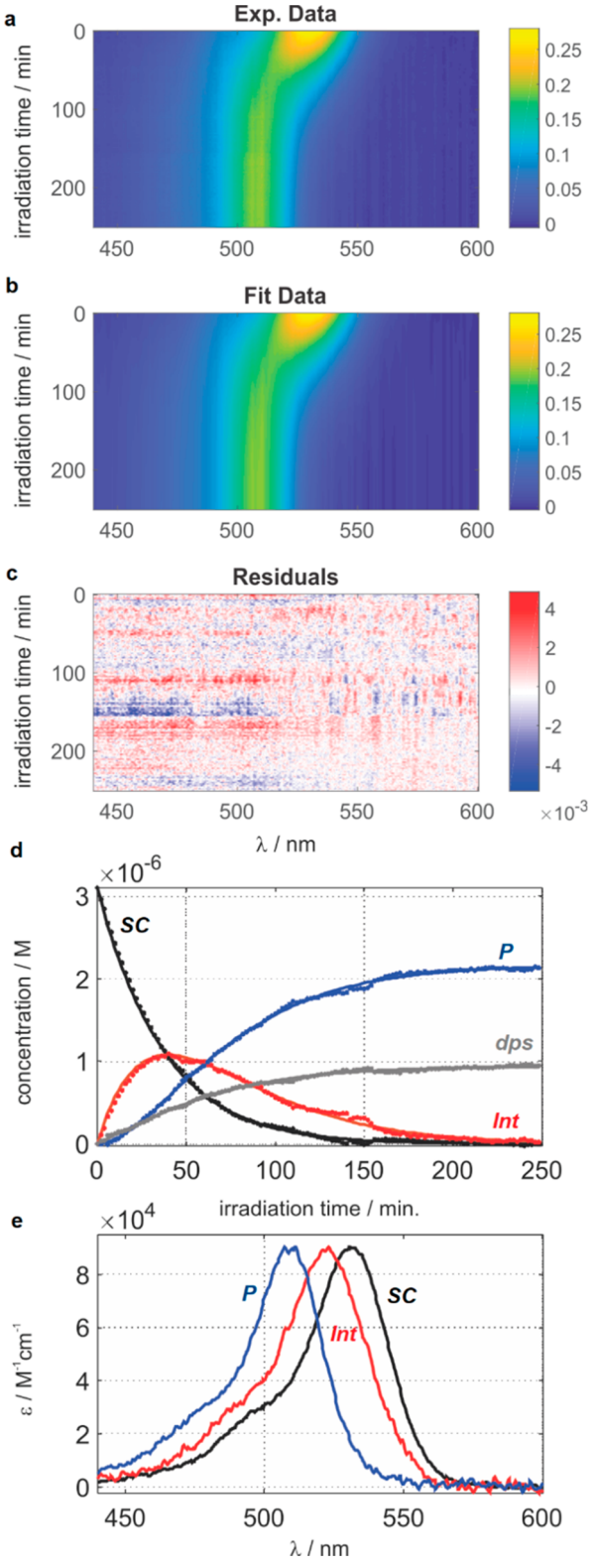

Figure 5. Photodegradation kinetics of **2h** simulated with the two-step photobluing model (model D, Scheme S3). (a) Experimental 2D data $A^{EXP}(\lambda,t)$; (b) fitted 2D data $A^{fit}(\lambda,t)$; (c) residuals map $A^{EXP}(\lambda,t) - A^{fit}(\lambda,t)$; (d) concentration profiles, assuming $\varepsilon(\lambda_{max}) = 9 \times 10^4$ M^{-1} cm^{-1} for all components, calculated from experimental (dots, $C = A^{EXP} \times E^{T}$) and fitted data (lines, $C = A^{fit} \times E^{T}$); (e) the resulting fitted absorption spectra matrix E. The corresponding fitted quantum yields for individual photoconversion processes are given in Table 1; dps, dark products.

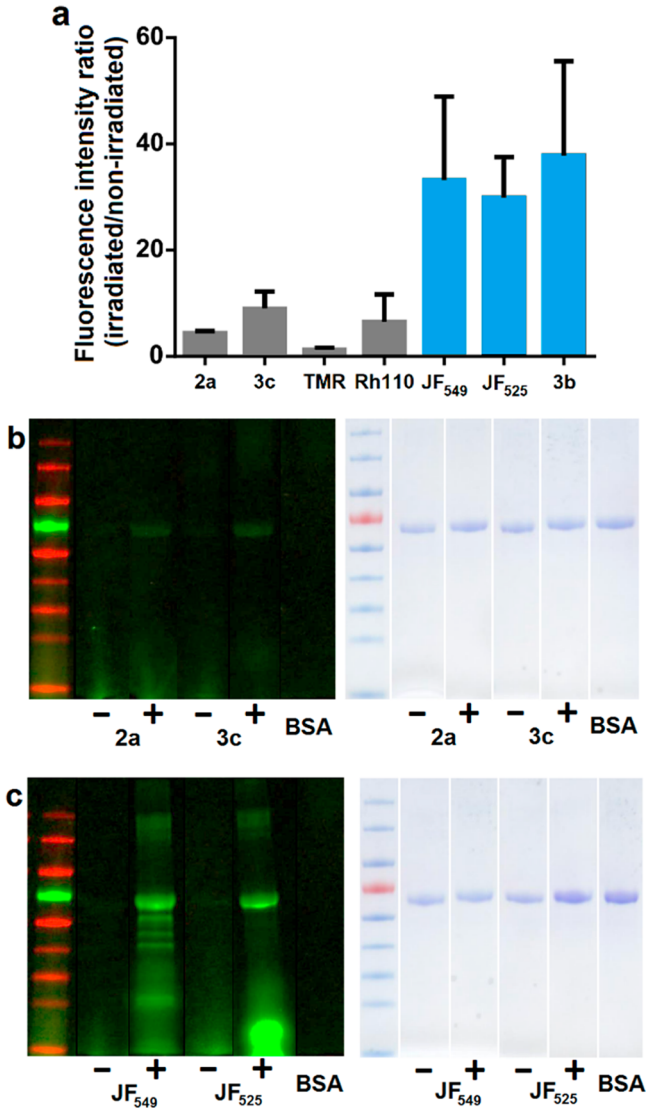

Figure 6. Quantification of nonspecific protein labeling with the fluorophore photooxidation products. (a) Solutions of fluorophores (10 μM in 0.1% (v/v) DMSO–PBS, pH 7.4, air-saturated) were irradiated with 525 nm LED array (300 W) at 30 °C in flow (residence time 5.1 min) followed by incubation with 1 mg/mL bovine serum albumin (BSA) in the dark (25 °C, 18 h). In control experiments, no irradiation was performed. The incubated samples were analyzed under denaturing contitions (SDS-PAGE), and the in-gel fluorescence was measured (Figure S32). Data points are presented as mean with standard deviation (N = 3). (b, c) Sample gel images with nonbluing (b) and bluing (c) fluorophores; − and + denote nonirradiated and irradiated dye samples, respectively.

The results of a sample analysis of the photobluing/photobleaching kinetics are shown in Figure 5. As is evident from the data in Table 1, and according to our expectations, the rhodamine fluorophores bearing a *tert*-alkyl substituent did not manifest appreciable photooxidative bluing effects. Rhodamine 110 showed similar spectral stability, and Foley's azabicycloheptane-substituted fluorophore **3c** and its hydrophilized analog **3d** were also resistant. On the contrary, most tetra- or *N*,*N*′-disubstituted rhodamines underwent dealkylative photooxidation with efficiencies comparable to those of the photobleaching process. In all cases, the isolated major intermediates in these photoreactions corresponded to the

DOI: 10.1021/jacs.8b11036
J. Am. Chem. Soc. 2019, 141, 981−989

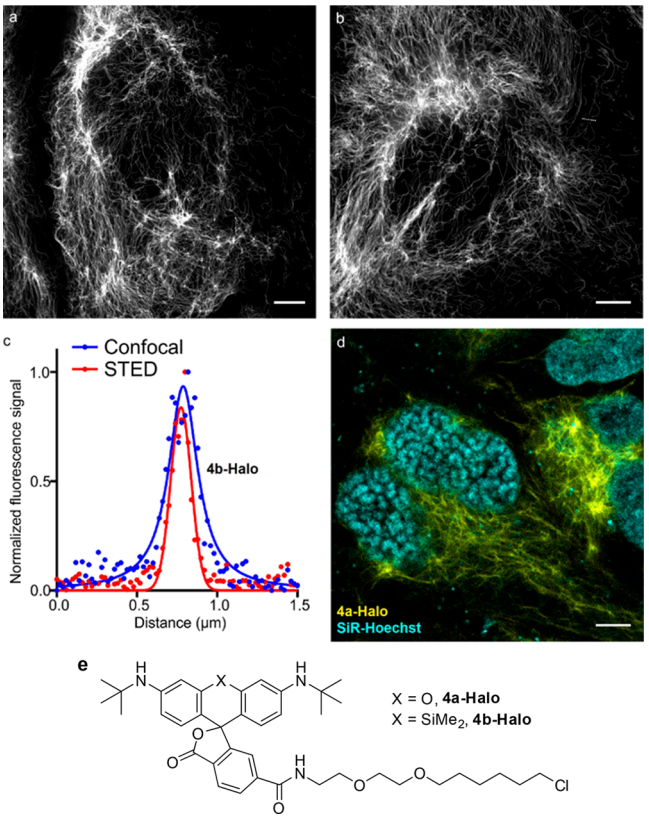

Figure 7. Images of living U2OS cells with stable expression of HaloTag-vimentin fusion protein stained with the indicated HaloTag fluorescent ligands. (a) STED image of living U2OS cells stained with 1 μM SiR-Halo[36] in Dulbecco's modified Eagle's medium (DMEM) at 37 °C for 1 h. (b) STED image of living U2OS cells stained with 1 μM **4b-Halo** in DMEM at 37 °C for 1 h. (c) Confocal and STED intensity profiles of the image shown in (b) panel at the positions indicated by the dotted line. (d) Confocal image of living U2OS cells stained with 1 μM **4a-Halo** and SiR-Hoechst[38] in DMEM at 37 °C for 1 h. (e) Chemical structures of the HaloTag ligands. In all cases, cells were washed once with Hank's balanced salt solution before imaging in DMEM; scale bars 5 μm.

products of stepwise *N*-dealkylation (Figure 1,a). These photoproducts were characterized whenever possible (Tables S6–S12); for example, we separated all five dealkylation products of Rhodamine B. In an experiment with exhaustive photodealkylation of Rhodamine B to Rhodamine 110 (corresponding to ~50 nm hypsochromic shifts of absorption and emission maxima), a minor *N*-substituent oxidation byproduct was identified as *N*-acetylrhodamine 110 (see Figure 1a, step v′).

For **3b**, a hemiaminal ether **3b-4** (Tables S11 and S12), arising from the trapping of a reactive trifluoroacetaldimmonium intermediate with the solvent, was also isolated; however, as we expected, the methyl and not the trifluoroethyl groups were predominantly subject to the oxidative cleavage (Figure 1c). It is also worth noting that, in most cases, when the photobluing pathway is open, the photooxidation of *N*-substituents is of comparable or higher efficiency to the destructive photobleaching (see the values $\Phi_{blue1}/\Phi_{bleach1} > 1$ in Table 1). The introduction of 2,2,2-trifluoroethyl substituents in **3b** (and fluorination of the azetidine substituents in JF_{525}) suppresses this relative predominance of photobluing ($\Phi_{blue1}/\Phi_{bleach1} < 1$).

The presence of hydroxyl groups[24b] in the β-positions of *tert*-alkyl substituents led to a pronounced increase in substituent photooxidation, resulting in the rapidly bluing dye **2h** and implying the fragmentation of the ensuing radical cation (Figure 1a, step ii) with the loss of formaldehyde. The hydroxylated analogues **2i,j** were considerably more resistant, likely due to additive $-I$ effects of multiple β-hydroxy substituents. More remote hydroxylation (in bridged cycles) was well tolerated, resulting in highly photo- and spectrally stable fluorophores **2g** and **3d**.

Photobluing fluorophores derived from cyclic secondary amines, such as JF_{525}[35] and JF_{549},[12b] represented a particular case. Photooxidative opening of azetidine substituents in JF_{549} must have proceeded via a highly reactive 1-azetinium intermediate, which (similarly to **3b**) then reacted with the nucleophilic solvent with formation of 2-ethoxyazetidine and finally 3-aminopropionaldehyde diethyl acetal products. Only the acetal products were sufficiently stable for identification in the mixture by LC–MS, yet upon attempted isolation they underwent extensive self-condensation. The formation of masked aldehyde was confirmed by trapping all three possible diethyl acetal photoproducts upon treatment with excess 2,4-dinitrophenylhydrazine (Table S13). Under identical conditions, the dye JF_{525} underwent quick and complex degradation explicable by much higher electrophilic reactivity of 2,2-difluoropropionaldehyde derivatives.

The electrophilic reactivity of the oxidative photobluing products of triarylmethane fluorophores may be of consequence for the long-term microscopy in live cells, as the reactive aldehyde species derived from fluorescent probes will contribute to unwanted and unexpected cross-reactivity with biomolecules. For instance, an off-target covalent labeling and intramolecular cross-linking of tagged proteins is to be anticipated. As an illustrative example, the dilute solutions of bluing and nonbluing rhodamine fluorophores were briefly irradiated in air-saturated aqueous phosphate-buffered saline (PBS) followed by incubation with bovine serum albumin in the dark. The SDS-PAGE analysis (Figure 6) of irradiated vs nonirradiated samples clearly showed that the bluing fluorophores forming reactive oxidation products (JF dyes and **3b**) were predisposed to formation of covalent fluorescent dye-protein adducts.

Sample Imaging Results with Nonbluing Fluorophores. To demonstrate the suitability of the newly introduced nonbluing analogues of triarylmethane fluorescent dyes for live-cell super-resolution imaging, we prepared the dyes **4a,b** as analogues of the validated live cell labels 520R[24a] and silico-rhodamine (SiR).[36] These were then converted to the cell-permeant self-labeling HaloTag ligands **4a,b-Halo** (Figure 7). The **4a-Halo** probe, although not compatible with 775 nm de-excitation, selectively stained the vimentin intermediate filaments in two-color confocal imaging of living human U2OS cells endogeneously expressing Vimentin-HaloTag fusion protein[37] and cotreated with SiR-Hoechst.[38] The spectrally stable SiR analog **4b-Halo** demonstrated similar image quality to SiR-Halo[36] in terms of target selectivity, contrast, background, and resolution in 775 nm live-cell STED nanoscopy.

■ CONCLUSION

Photoconversion of widely used triarylmethane fluorophores results in a series of photooxidative transformations. The photooxidation products demonstrate hypsochromic absorp-

DOI: 10.1021/jacs.8b11036
J. Am. Chem. Soc. 2019, 141, 981–989

tion and emission shifts and are accumulated with rates intrinsically dependent on the *N*-substitution pattern of a given fluorophore. Moreover, the photostability of the photoconversion intermediates also varies on a case-by-case basis. As the spectral stability of fluorescent labels is critical to identification and tracking of the observed objects in multicolor super-resolution and, in particular, in single-molecule imaging, choosing the nonbluing fluorescent labels will be essential for the robustness of data analysis, integrity, and reproducibility in such applications. Of particular note is the demonstrated generation of chemically reactive species upon photooxidation of rhodamine labels with cyclic dialkylamino substituents. Under live-cell imaging conditions, these photoproducts may form covalent fluorescent adducts with off-target biomolecules and, therefore, alter the expected selectivity of employed fluorescent ligands.

Using the sequential Ru- and Cu-catalyzed transformations, we have prepared a series of nonbluing *N,N′*-di-*tert*-alkylrhodamine fluorophores with diverse substitution patterns and validated them as intact cell membrane-permeant labels. Besides *tert*-alkylamino groups, we have identified unsubstituted amino, (2,2,2-trifluoroethyl)amino, and 7-azabicyclo[2.2.1]heptyl auxochromic substituents as providing the spectrally stable triarylmethane fluorophores. Along with the proper choice of the bridging group (O, CMe_2, $SiMe_2$), these substitution options will allow for sufficient spectral diversity of the fluorophores and, by extension, can be recommended for future development of other types of fluorescent labels for demanding multicolor bioimaging applications.

■ ASSOCIATED CONTENT

Supporting Information

The Supporting Information is available free of charge on the ACS Publications website at DOI: 10.1021/jacs.8b11036.

Synthetic procedures and characterizations of the compounds, description of the flow photoreactor, photochemical experiments, and data analysis, including Figures S1−S32, Tables S1−S13, and Schemes S1−S4 (PDF)

NMR spectra (PDF)

■ AUTHOR INFORMATION

Corresponding Authors

*alexey.butkevich@mpibpc.mpg.de

*stefan.hell@mpibpc.mpg.de

ORCID

Alexey N. Butkevich: 0000-0002-9885-6434

Gražvydas Lukinavičius: 0000-0002-7176-1793

Stefan W. Hell: 0000-0002-9638-5077

Notes

The authors declare the following competing financial interest(s): G.L. has filed a patent application on the SiR fluorophore.

■ ACKNOWLEDGMENTS

Financial support of this project by the Max Planck Society as well as an Erwin Neher Fellowship (to A.N.B.) and a Nobel Laureate Fellowship (to G.L.) are greatly appreciated. The authors thank Mario Lengauer, Rainer Schürkötter, and the staff of Precision Mechanics Workshop (MPI BPC), Frank Meyer, Julian Janssen, and the staff of IT & Electronics Service (MPI BPC) for building the flow photoreactor; Rainer Pick, Jaydev Jethwa, and Dr. Ellen Rothermel for technical assistance; Tanja Gilat for cell culturing; and Dr. Gyuzel Y. Mitronova for the samples of HaloTag(O2) amine and **3b-3** dye. We are also grateful to Jürgen Bienert (MPI BPC) and Holm Frauendorf and co-workers (Georg-August-Universität Göttingen) for recording MS and NMR spectra and to Dr. Vladimir N. Belov for proofreading the manuscript.

■ REFERENCES

(1) Sahl, S. J.; Hell, S. W.; Jakobs, S. Fluorescence nanoscopy in cell biology. *Nat. Rev. Mol. Cell Biol.* **2017**, *18*, 685−701.

(2) Curthoys, N. M.; Parent, M.; Mlodzianoski, M.; Nelson, A. J.; Lilieholm, J.; Butler, M. B.; Valles, M.; Hess, S. T. Dances with membranes: breakthroughs from super-resolution imaging. *Curr. Top. Membr.* **2015**, *75*, 59−123.

(3) (a) Bottanelli, F.; Kromann, E. B.; Allgeyer, E. S.; Erdmann, R. S.; Wood Baguley, S.; Sirinakis, G.; Schepartz, A.; Baddeley, D.; Toomre, D. K.; Rothman, J. E.; Bewersdorf, J. Two-colour live-cell nanoscale imaging of intracellular targets. *Nat. Commun.* **2016**, *7*, 10778. (b) Lukinavičius, G.; Reymond, L.; Umezawa, K.; Sallin, O.; D'Este, E.; Göttfert, F.; Ta, H.; Hell, S. W.; Urano, Y.; Johnsson, K. Fluorogenic probes for multicolor imaging in living cells. *J. Am. Chem. Soc.* **2016**, *138*, 9365−9368.

(4) Dean, K. M.; Palmer, A. E. Advances in fluorescence labeling strategies for dynamic cellular imaging. *Nat. Chem. Biol.* **2014**, *10*, 512−523.

(5) Butkevich, A. N.; Lukinavičius, G.; D'Este, E.; Hell, S. W. Cell-permeant large Stokes shift dyes for transfection-free multicolor nanoscopy. *J. Am. Chem. Soc.* **2017**, *139*, 12378−12381.

(6) Winter, F. R.; Loidolt, M.; Westphal, V.; Butkevich, A. N.; Gregor, C.; Sahl, S. J.; Hell, S. W. Multicolour nanoscopy of fixed and living cells with a single STED beam and hyperspectral detection. *Sci. Rep.* **2017**, *7*, 46492.

(7) Niehörster, T.; Löschberger, A.; Gregor, I.; Krämer, B.; Rahn, H.-J.; Patting, M.; Koberling, F.; Enderlein, J.; Sauer, M. Multi-target spectrally resolved fluorescence lifetime imaging microscopy. *Nat. Methods* **2016**, *13*, 257−262.

(8) Garbacik, E. T.; Sanz-Paz, M.; Borgman, K. J. E.; Campelo, F.; Garcia-Parajo, M. F. Frequency-encoded multicolor fluorescence imaging with single-photon-counting color-blind detection. *Biophys. J.* **2018**, *115*, 725−736.

(9) Ha, T.; Tinnefeld, P. Photophysics of fluorescent probes for single-molecule biophysics and super-resolution imaging. *Annu. Rev. Phys. Chem.* **2012**, *63*, 595−617.

(10) Eggeling, C.; Widengren, J.; Rigler, R.; Seidel, C. A. M. Photobleaching of fluorescent dyes under conditions used for single-molecule detection: evidence of two-step photolysis. *Anal. Chem.* **1998**, *70*, 2651−2659.

(11) Go, Y. M.; Jones, D. P. Redox compartmentalization in eukaryotic cells. *Biochim. Biophys. Acta, Gen. Subj.* **2008**, *1780*, 1273−1290.

(12) (a) Podgorski, K.; Terpetschnig, E.; Klochko, O. P.; Obukhova, O. M.; Haas, K. Ultra-bright and -stable red and near-infrared squaraine fluorophores for *in vivo* two-photon imaging. *PLoS One* **2012**, *7*, No. e51980. (b) Grimm, J. B.; English, B. P.; Chen, J.; Slaughter, J. P.; Zhang, Z.; Revyakin, A.; Patel, R.; Macklin, J. J.; Normanno, D.; Singer, R. H.; Lionnet, T.; Lavis, L. D. A general method to improve fluorophores for live-cell and single-molecule microscopy. *Nat. Methods* **2015**, *12*, 244−250. (c) Patalag, L. J.; Ho, L. P.; Jones, P. G.; Werz, D. B. Ethylene-bridged oligo-BODIPYs: access to intramolecular J-aggregates and superfluorophores. *J. Am. Chem. Soc.* **2017**, *139*, 15104−15113.

(13) (a) Zheng, Q.; Juette, M. F.; Jockusch, S.; Wasserman, M. R.; Zhou, Z.; Altman, R. B.; Blanchard, S. C. Ultra-stable organic fluorophores for single-molecule research. *Chem. Soc. Rev.* **2014**, *43*, 1044−1056. (b) Zheng, Q.; Jockusch, S.; Zhou, Z.; Altman, R. B.;

DOI: 10.1021/jacs.8b11036
J. Am. Chem. Soc. 2019, 141, 981−989

Zhao, H.; Asher, W.; Holsey, M.; Mathiasen, S.; Geggier, P.; Javitch, J. A.; Blanchard, S. C. Electronic tuning of self-healing fluorophores for live-cell and single-molecule imaging. *Chem. Sci.* **2017**, *8*, 755−762.
(14) Evans, N. A. Photofading of rhodamine dyes. II. Photodealkylation of rhodamine B. *J. Soc. Dyers Colour.* **1973**, *89*, 332.
(15) (a) Li, X.; Liu, G.; Zhao, J. Two competitive primary processes in the photodegradation of cationic triarylmethane dyes under visible irradiation in TiO_2 dispersions. *New J. Chem.* **1999**, *23*, 1193−1196. (b) Chen, C.-C.; Lu, C.-S.; Mai, F.-D.; Weng, C.-S. Photooxidative *N*-de-ethylation of anionic triarylmethane dye (sulfan blue) in titanium dioxide dispersions under UV irradiation. *J. Hazard. Mater.* **2006**, *137*, 1600−1607.
(16) (a) Winters, B. H.; Mandelberg, H. I.; Mohr, W. B. Photochemical products in coumarin laser dyes. *Appl. Phys. Lett.* **1974**, *25*, 723−725. (b) Kuznetsova, N. A.; Kaliya, O. L. The photochemistry of coumarins. *Russ. Chem. Rev.* **1992**, *61*, 683−696.
(17) (a) Smith, P. J.; Mann, C. K. Electrochemical dealkylation of aliphatic amines. *J. Org. Chem.* **1969**, *34*, 1821−1826. (b) Portis, L. C.; Bhat, V. V.; Mann, C. K. Electrochemical dealkylation of aliphatic tertiary and secondary amines. *J. Org. Chem.* **1970**, *35*, 2175−2178.
(18) Liu, F.; Zhang, Z.; Bao, Z.; Su, B.; Xing, H.; Yang, Q.; Yang, Y.; Ren, Q. Visible-light-mediated dealkylative coupling of trialkylamines with dialkyl acetylenedicarboxylates. *Synlett* **2017**, *28*, 1116−1120.
(19) Liao, Z.; Bogh, S. A.; Santella, M.; Rein, C.; Sørensen, T. J.; Laursen, B. W.; Vosch, T. Emissive photoconversion products of an amino-triangulenium dye. *J. Phys. Chem. A* **2016**, *120*, 3554−3561.
(20) Jones, G., II; Bergmark, W. R.; Jackson, W. R. Products of photodegradation for coumarin laser dyes. *Opt. Commun.* **1984**, *50*, 320−323.
(21) Song, X.; Johnson, A.; Foley, J. 7-Azabicyclo[2.2.1]heptane as a unique and effective dialkylamino auxochrome moiety: demonstration in a fluorescent rhodamine dye. *J. Am. Chem. Soc.* **2008**, *130*, 17652−17653.
(22) Liu, X.; Qiao, Q.; Tian, W.; Liu, W.; Chen, J.; Lang, M. J.; Xu, Z. Aziridinyl fluorophores demonstrate bright fluorescence and superior photostability by effectively inhibiting twisted intramolecular charge transfer. *J. Am. Chem. Soc.* **2016**, *138*, 6960−6963.
(23) (a) Mitronova, G. Y.; Belov, V. N.; Bossi, M. L.; Wurm, C. A.; Meyer, L.; Medda, R.; Moneron, G.; Bretschneider, S.; Eggeling, C.; Jakobs, S.; Hell, S. W. New fluorinated rhodamines for optical microscopy and nanoscopy. *Chem. - Eur. J.* **2010**, *16*, 4477−4488. (b) Belov, V. N.; Mitronova, G. Y.; Bossi, M. L.; Boyarskiy, V. P.; Hebisch, E.; Geisler, C.; Kolmakov, K.; Wurm, C. A.; Willig, K. I.; Hell, S. W. Masked rhodamine dyes of five principal colors revealed by photolysis of a 2-diazo-1-indanone caging group: synthesis, photophysics, and light microscopy applications. *Chem. - Eur. J.* **2014**, *20*, 13162−13173.
(24) (a) Butkevich, A. N.; Mitronova, G. Y.; Sidenstein, S. C.; Klocke, J. L.; Kamin, D.; Meineke, D. N. H.; D'Este, E.; Kraemer, P.-T.; Danzl, J. G.; Belov, V. N.; Hell, S. W. Fluorescent rhodamines and fluorogenic carbopyronines for super resolution STED microscopy in living cells. *Angew. Chem., Int. Ed.* **2016**, *55*, 3290−3294. (b) Butkevich, A. N.; Belov, V. N.; Kolmakov, K.; Sokolov, V. V.; Shojaei, H.; Sidenstein, S. C.; Kamin, D.; Matthias, J.; Vlijm, R.; Engelhardt, J.; Hell, S. W. Hydroxylated fluorescent dyes for live cell labeling: synthesis, spectra and super resolution STED microscopy. *Chem. - Eur. J.* **2017**, *23*, 12114−12119.
(25) Grimm, J. B.; Lavis, L. D. Synthesis of rhodamines from fluoresceins using Pd-catalyzed C−N cross-coupling. *Org. Lett.* **2011**, *13*, 6354−6357.
(26) (a) Jiang, J.; Zhu, H.; Shen, Y.; Tu, T. Acenaphthoimidazolium chloride-enabled nickel-catalyzed amination of bulky aryl tosylates. *Org. Chem. Front.* **2014**, *1*, 1172−1175. (b) Ruiz-Castillo, P.; Blackmond, D. G.; Buchwald, S. L. Rational ligand design for the arylation of hindered primary amines guided by reaction progress kinetic analysis. *J. Am. Chem. Soc.* **2015**, *137*, 3085−3092.
(27) Dennis, J. M.; White, N. A.; Liu, R. Y.; Buchwald, S. L. Breaking the base barrier: an electron-deficient palladium catalyst enables the use of a common soluble base in C−N coupling. *J. Am. Chem. Soc.* **2018**, *140*, 4721−4725.
(28) Sambiagio, C.; Marsden, S. P.; Blacker, A. J.; McGowan, P. C. Copper catalysed Ullmann type chemistry: from mechanistic aspects to modern development. *Chem. Soc. Rev.* **2014**, *43*, 3525−3550.
(29) Imazaki, Y.; Shirakawa, E.; Ueno, R.; Hayashi, T. Ruthenium-catalyzed transformation of aryl and alkenyl triflates to halides. *J. Am. Chem. Soc.* **2012**, *134*, 14760−14763.
(30) Price (October 2018, Strem Chemicals, Inc.): $[Cp^*Ru(MeCN)_3]OTf$, \$384/g, $[Cp^*RuCl_2]_n$, \$90/g. $[Cp^*RuCl_2]_n$ is also accessible in a one-step reaction from Cp*H and $RuCl_3 \cdot xH_2O$; see: Koelle, U.; Kossakowski, J.; Grumbine, D.; Tilley, T. D. Di μ chloro bis[(η^5 pentamethylcyclopentadienyl) chlororuthenium(III)], $[Cp^*RuCl_2]_2$ and di μ methoxo bis(η^5 pentamethylcyclopentadienyl)-diruthenium(II), $[Cp^*RuOMe]_2$. *Inorg. Synth.* **2007**, *29*, 225−228.
(31) Konovalov, A. I.; Gorbacheva, E. O.; Miloserdov, F. M.; Grushin, V. V. Ruthenium-catalyzed nucleophilic fluorination of halobenzenes. *Chem. Commun.* **2015**, *51*, 13527−13530.
(32) Beyzavi, M. H.; Mandal, D.; Strebl, M. G.; Neumann, C. N.; D'Amato, E. M.; Chen, J.; Hooker, J. M.; Ritter, T. ^{18}F-Deoxyfluorination of phenols via Ru π-complexes. *ACS Cent. Sci.* **2017**, *3*, 944−948.
(33) Ding, X.; Huang, M.; Yi, Z.; Du, D.; Zhu, X.; Wan, Y. Room-temperature CuI-catalyzed amination of aryl iodides and aryl bromides. *J. Org. Chem.* **2017**, *82*, 5416−5423.
(34) Marcolongo, J. P.; Schmidt, J.; Levin, N.; Slep, L. D. A chemometric approach for determining the reaction quantum yields in consecutive photochemical processes. *Phys. Chem. Chem. Phys.* **2017**, *19*, 21373−21381.
(35) Grimm, J. B.; Muthusamy, A. K.; Liang, Y.; Brown, T. A.; Lemon, W. C.; Patel, R.; Lu, R.; Macklin, J. J.; Keller, P. J.; Ji, N.; Lavis, L. D. A general method to fine-tune fluorophores for live-cell and in vivo imaging. *Nat. Methods* **2017**, *14*, 987−994.
(36) Lukinavičius, G.; Umezawa, K.; Olivier, N.; Honigmann, A.; Yang, G.; Plass, T.; Mueller, V.; Reymond, L.; Corrêa, I. R., Jr.; Luo, Z.-G.; Schultz, C.; Lemke, E. A.; Heppenstall, P.; Eggeling, C.; Manley, S.; Johnsson, K. A near-infrared fluorophore for live-cell super-resolution microscopy of cellular proteins. *Nat. Chem.* **2013**, *5*, 132−139.
(37) Butkevich, A. N.; Ta, H.; Ratz, M.; Stoldt, S.; Jakobs, S.; Belov, V. N.; Hell, S. W. Two-color 810 nm STED nanoscopy of living cells with endogenous SNAP-tagged fusion proteins. *ACS Chem. Biol.* **2018**, *13*, 475−480.
(38) Lukinavičius, G.; Blaukopf, C.; Pershagen, E.; Schena, A.; Reymond, L.; Derivery, E.; Gonzalez-Gaitan, M.; D'Este, E.; Hell, S. W.; Gerlich, D. W.; Johnsson, K. SiR−Hoechst is a far-red DNA stain for live-cell nanoscopy. *Nat. Commun.* **2015**, *6*, 8497.

DOI: 10.1021/jacs.8b11036
J. Am. Chem. Soc. 2019, 141, 981−989